Journal of Sound and Vibration 590 (2024) 118544

Contents lists available at ScienceDirect

Journal of Sound and Vibration

journal homepage: www.elsevier.com/locate/jsvi

Building functional networks for complex response analysis in systems of coupled nonlinear oscillators

Charlotte Geier [a,*], Merten Stender [b], Norbert Hoffmann [a,c]

[a] Hamburg University of Technology, Department of Mechanical Engineering, Am Schwarzenberg-Campus 1, Hamburg, 21073, Germany
[b] Chair of Cyber-Physical Systems in Mechanical Engineering, Technische Universität Berlin, Straße des 17. Juni 135, Berlin, 10623, Germany
[c] Imperial College London, Mechanical Engineering, Exhibition Road, London, SW7 2AZ, UK

ARTICLE INFO

Keywords:
Complex networks
Nonlinear dynamics
Time series analysis
Synchronization
Transient analysis
Duffing oscillators

ABSTRACT

Some aspects of engineering dynamics, such as nonlinearities and transient motion of many interconnected parts, remain difficult to handle today. To comply with increasing demands on resilience and safety, the dynamics of large machines need to be better understood. Complex network methods, already present in many scientific disciplines, provide a tool set complementary to conventional methods of system analysis. This work aims at providing a new, function-based view on mechanical systems by generating functional networks. To this end, a network algorithm is applied to sets of cyclically coupled Duffing oscillators as a common example of a complex nonlinear mechanical system. In the functional network, each node represents an oscillator while the direction of the network edges represents a functional coupling. Results show that the network method is capable of identifying dynamical transitions and synchronization between components, as well as determining the number of different states present within a system. Additionally, the time evolution of the component interactions, especially in response to a disturbance, is studied via a sliding-window approach. The results of this analysis might hopefully open new ways for a more efficient system analysis through optional sensor placement, and for effective countermeasures against unwanted dynamics through improved analysis of transient dynamics.

1. Introduction

Engineering dynamics studies large machines, which consist of many connected moving parts. The analysis of these systems is often challenging in practice [1]. Large deformations of machine parts [2], joints [3], friction [4,5], or material nonlinearities [6,7] cause nonlinear effects. These nonlinearities, as well as transient loads and motion, combined with a large number of degrees of freedom, still pose challenges to state-of-the-art system understanding and modeling approaches. At the same time, the need for lightweight structures that can withstand large and unsteady environmental loads is growing. Examples of such structures are offshore wind turbines, satellites, and space antennas. To avoid unwanted and potentially harmful vibrations, for example, in the blade of a turbine, a deeper understanding of the dynamics of these systems becomes crucial. Transfer path analysis [8] and operational deflection shape analysis [9] provide a tool set for studying the dynamics of composed structures. The accuracy of the former relies on accurate measurements and suitable sensor placement to collect appropriate data for the analysis [10]. Despite the available techniques, the identification and analysis of functional dependencies, and especially the study of transient motion, remain challenging for engineers. This work provides a complementary view of these issues in structural machine dynamics by

* Corresponding author.
E-mail address: charlotte.geier@tuhh.de (C. Geier).

https://doi.org/10.1016/j.jsv.2024.118544
Received 1 December 2023; Received in revised form 27 May 2024; Accepted 28 May 2024
Available online 30 May 2024
0022-460X/© 2024 The Author(s). Published by Elsevier Ltd. This is an open access article under the CC BY license (http://creativecommons.org/licenses/by/4.0/).

representing the mechanical structure as an alternative network model. Classical, geometry-based models represent these mechanical systems as components which are connected via springs and dampers based on their geometrical coupling or, in other words, their geometrical proximity. In our functional networks, each node also represents a component of the mechanical structure. In contrast to the mechanical model, the edges of the network represent functional interrelations obtained from a network-based approach. These functional interrelations are based on the dynamical interaction of the components, instead of their geometrical proximity. This approach opens the door for a variety of new network-based tools.

Network methods are popular in many fields of science, such as mathematics, physics, biology, computer science, the social sciences, medicine, and climate research [11–15]. Common examples of networks include the internet, neural networks [16], social networks [11], or power grids [17,18]. The investigation of dynamical systems as a network provides complementary tools for time series analysis [11,15] by generating a network from (measurement) time series data. This transformation from time- to network domain makes it possible to study the time series through the properties of the resulting network [19,20]. Based on this approach, network analysis has been used to identify coupling properties between different system components of a dynamical system [21–23], detect anomalies [24] and distinguish various dynamical states [25–28]. Aspects of transient motion of the system can be studied in the network domain, such as regime changes [29] and types of synchronization [28,30–33]. A detailed review of network methods for the study of dynamical systems and their possibilities can be found in [15].

In this work, network analysis with the inter-system recurrence network (ISRN) method [21] is applied to a classical toy model for a mechanical systems, a set of coupled Duffing oscillators, to generate a functional network. ISRN analysis has been used to identify the direction of links between two weakly coupled Rössler systems and to study the interrelation between two paleoclimate time series in [21], making it an appealing candidate for analyzing the functional dependencies between distinct components. The nonlinear Duffing oscillator, or sets of coupled Duffing oscillators, are a model system in many engineering applications such as forced coupled pendulums [34], alternating current electric fields [35], or vibrating bladed discs [2,36–38] which exist for example in aircraft or wind turbines [2]. The obtained functional network is then used to study functional dependencies within the mechanical system at different dynamical states, as well as the evolution of the network structure during transient processes.

The remainder of this work is structured as follows: In Section 2, the model system used in this study is presented, followed by an introduction of the applied network methods in Section 3. Section 4 includes the results for the functional network and analysis of a transient system. A discussion of the results is provided in Section 5. The paper closes with a conclusion in Section 6.

2. Coupled duffing oscillators

The Duffing oscillator is a well-known dynamical system whose dynamics have been described extensively in several works [36, 39,40]. In engineering, a single Duffing oscillator represents a common model for systems with nonlinearities due to material nonlinearities, or large deformations or motions. Example of these systems are a nonlinear pendulum [34], systems with a nonlinear spring [2] or a single blade [2,36–38]. More complex structures such as bladed disks in turbines, wind turbines, or space antennas, can be modeled by coupling several Duffing oscillators [2]. In these models, one machine component can be represented by a single oscillator. The Duffing oscillator exhibits rich dynamical behavior [36,39–41]. For specific parameter combinations, the single oscillator exhibits bi-stability [2,39], and chaotic behavior [39,40]. Correspondingly, sets of coupled oscillators may exhibit multi-stability. The bi- or multi-stability property can give rise to potentially harmful localized vibrations in coupled systems [2], where a single oscillator or a group of oscillators vibrates at a much higher amplitude than the overall system. In practice, this phenomenon can lead to system failure, for example if a turbine blade breaks due to high stress induced by high-amplitude oscillations.

A single, forced Duffing oscillator [39] is described by

$$m\ddot{x} + d\dot{x} + k_\mathrm{l}x + k_\mathrm{nl}x^3 = f(t), \tag{1}$$

where m is the model mass, d the damping coefficient, k_l and k_nl the linear and nonlinear spring stiffness. The system displacement is given by x, its velocity by the time derivative $\dot{x}$ and the acceleration by $\ddot{x}$. The forcing $f(t) = F\cos(\Omega t)$ is defined as harmonic forcing with amplitude F and angular frequency Ω. The damping is defined as Rayleigh damping $d = \alpha m + \beta k_\mathrm{l}$ with mass- and spring-proportional factors α and β, respectively. In this work, the parameter values are chosen such that the system exhibits bi-stability and the excitation frequency lies in the bi-stable regime. An overview of the parameters is given in Table 1. Fig. 1 illustrates the bi-stability behavior and hysteresis of the system for the given parameter settings. When the forcing frequency Ω is increased from zero, the amplitude $\hat{x}$ of the system response follows the path marked by red triangles and increases to $\hat{x} = 1.72$ m at $\Omega = 2.17$ rad s^{-1}, where it suddenly drops to values around $\hat{x} = 0.3$ m. On the other hand, if the forcing frequency is decreased, the amplitude follows the lower branch, marked by blue crosses, and jumps to a higher value of $\hat{x} = 1.55$ m at $\Omega = 1.89$ rad s^{-1}. The area between $1.89 < \Omega < 2.17$ rad s^{-1} defines the bi-stability region. In this work, the oscillator is excited at a frequency $\Omega = 2$ rad s^{-1} within that region, marked by a black dashed line. The right panel of Fig. 1 shows the time response of the Duffing oscillator with the given parameter settings for two different initial conditions. The initial conditions are defined as $\boldsymbol{x}_0 = [x_0, v_0]$, where x_0 is the initial displacement and v_0 is the initial velocity of the oscillator. When starting from $\boldsymbol{x}_{0,1} = [1, 0]$, the mass oscillates with a much higher amplitude than when starting at $\boldsymbol{x}_{0,2} = [0.1, 0]$.

For the purpose of studying a mechanical system made of several oscillators through a functional network, a system of $M = 5$ cyclically coupled Duffing oscillators with nearest-neighbor coupling is implemented, see Fig. 2. Similar systems are used as minimal models in engineering to model bladed disks, as described in [2,36,42]. The equation of motion for the nth oscillator is given by

$$m\ddot{x}_n + d\dot{x}_n + k_\mathrm{l}x_n - k_\mathrm{c}(x_{n-1} + x_{n+1} - 2x_n) + k_\mathrm{nl}x_n^3 = f(t), \tag{2}$$

Table 1
Model parameters. Overview of the model parameters used in this study, unless specified otherwise.

Measure	Symbol	Unit	Value
Mass	m	kg	1
Damping prop m	α	s^{-1}	0.1
Damping prop k	β	s	0
Linear spring	k_l	N m^{-1}	1
Nonlinear spring	k_{nl}	N m^{-3}	2
Coupling spring	k_c	N m^{-1}	0.1
Forcing amplitude	F	N	1
Forcing frequency	Ω	rad s^{-1}	2

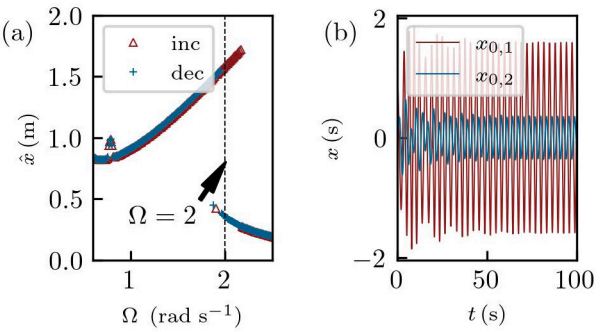

Fig. 1. Duffing oscillator with given parameter settings. The amplitude of the system response $\hat{x}$ follows two different paths for an upward- (red triangles) and downward (blue crosses) frequency sweep over the forcing frequency Ω. The bi-stability region is located at $\Omega = [1.89, 2.17]$ rad s^{-1}, where two stable solutions exist. The dashed line marks the chosen excitation frequency $\Omega = 2$ rad s^{-1}. On the right, the system responses for two different initial conditions $\boldsymbol{x}_{0,1} = [1, 0]$ (red), $\boldsymbol{x}_{0,2} = [0.1, 0]$ (blue) are shown, illustrating the dependence of the oscillation amplitude and phase on the initial conditions. (For interpretation of the references to color in this figure legend, the reader is referred to the web version of this article.)

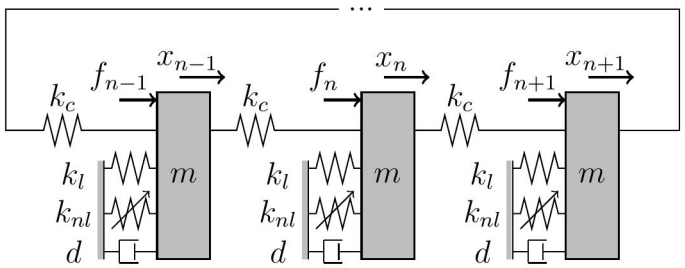

Fig. 2. Model system composed of a chain of $M = 5$ cyclically components. Each component is represented by a Duffing oscillators with nearest-neighbor coupling. The figure shows a only section of the entire model, using three oscillators to illustrate the nearest-neighbor coupling. The system is described by model masses m, the Rayleigh damping $d = \alpha m + \beta k_l$, linear and nonlinear springs k_l and k_{nl} and the connecting linear springs k_c. The displacement is given by x_n, and each mass is driven by an harmonic forcing $f_n(t) = F\cos(\Omega t)$.

where k_c describes the linear nearest-neighbor coupling spring. These types of coupled systems are known to exhibit complex dynamic behavior, such as nonlinear vibration localization [2], where a subsystem oscillates with much higher amplitude than the remainder of the system. This phenomenon is known to be caused by manufacturing imperfections (mistuning), but has also been shown to arise in fully homogeneous and symmetric structures due to bifurcations [2], as is the case for the model system at hand. The resulting high-amplitude oscillations cause a large amount of stress in the affected system components. This stress can lead to component and even system failure. Localization is therefore a potentially harmful phenomenon in the engineering context [2].

Eight different dynamical states of the five-oscillator system are studied, see Fig. 3. Each panel shows the dynamics of the entire five-oscillator system over time. Within a panel, a row represents a single oscillator of the system and the x-axis represents time. The deflection of each mass is mapped to a color bar. The first four states (a) to (d) are achieved solely by variation of the initial conditions, while the latter four (e) to (h) require variations from the system parameters in Table 1. The states in (a) and (b) show a uniform motion with all oscillators in low or high amplitude, respectively. Panels (c) and (d) show localized harmonic vibrations with one and three masses at high amplitudes, while all other masses vibrate at low amplitudes. Localized vibrations with higher periods are achieved by increasing the forcing amplitude to $F = 35$ N, see panels (e) and (f). By changing the forcing frequency from well within the bi-stability region to values at the border regions $\Omega = 1.873$ rad s^{-1} in panel (g) and $\Omega = 2.295$ rad s^{-1} in panel (h), fronts are created [43], which propagate a specific state depending on the initial conditions. The initial conditions are presented in the Appendix.

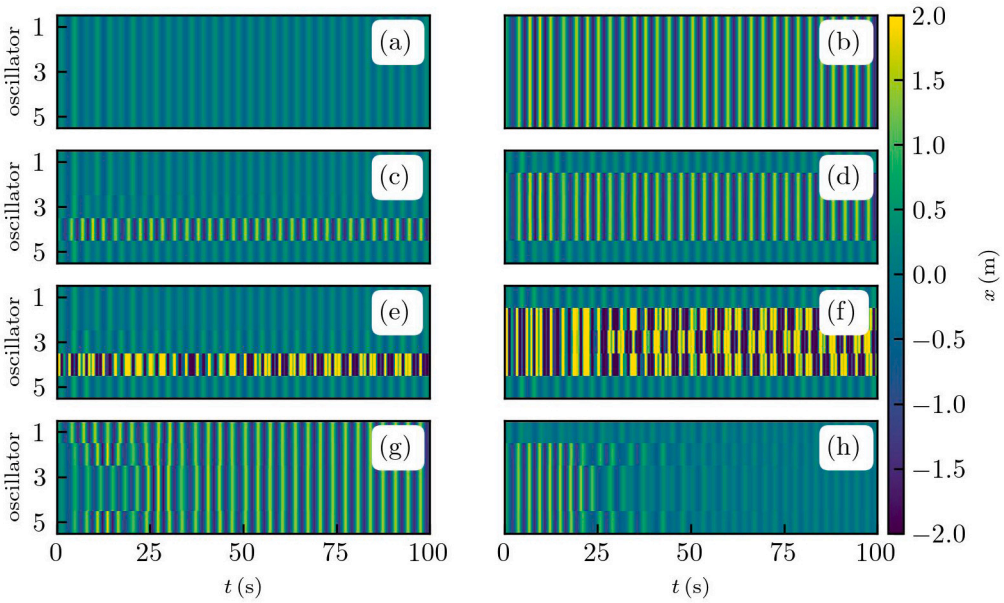

Fig. 3. Dynamics of the Duffing oscillator chain with $M = 5$ masses. The system parameters are as listed in Table 1, unless specified otherwise. (a) uniform oscillation at low amplitude, (b) uniform oscillation at high amplitude, (c) localized harmonic vibration: one oscillator with high amplitude, (d) localized harmonic vibration: three oscillators with high amplitudes, (e) localized higher-periodic oscillation: one oscillator in higher-periodic oscillation, where $F_4 = 35$ N, (f) localized higher-periodic oscillation: of three oscillators, where $F_{2,3,4} = 35$ N, (g) transient motion: front at lower end of bi-stability region, where $\Omega = 1.873$ rad s^{-1} and (h) transient motion: front at upper end of bi-stability region, where $\Omega = 2.295$ rad s^{-1}. The initial conditions $\boldsymbol{x}_{0,i}$ for the ith case are given in the Appendix. (For interpretation of the references to color in this figure legend, the reader is referred to the web version of this article.)

Although the studies in this work are limited to a homogeneous system composed of components with two states each, the approach would be equally valid for a system with components with any number of states, or even a heterogeneous system where the individual components have different numbers of states. The method focuses on the analysis of time series data, which could also be obtained from a system described by a partial differential equation, as long as a discretized time series is available.

The time series data used in the following studies is generated by integrating Eq. (2) using the integrator 'dopri5' in Python Scipy [44]. 'Dopri5' is an explicit Runge–Kutta method of order 4(5) with step size control and dense output [45]. The resulting time series have a length of $t = 100$ s and are discretized with a step size of $dt = 0.05$ s.

There is a large variety of well-established tools that can be employed to study data from complex nonlinear models. Most of these methods are based in time- or frequency domain. This work aims at building a complementary perspective, given by a functional network. This alternative view on the dynamics of a mechanical system focuses on functional dynamical relationships rather than geometrical proximity. The following section introduces the inference of functional networks based on a specific network algorithm, the inter-system recurrence network.

3. Inter-system recurrence networks and functional networks inference

In recent years, a number different methods for inferring networks from time series have been developed [15]. One group of methods are recurrence-based networks (RN) [46–50], which generate a network based on the mutual proximity of two observations in phase space. A particular recurrence-based network algorithm for the study of bi-variate data is the inter-system-recurrence network (ISRN) [15,21], which is the subject of this study. This section is dedicated to introducing the idea of RN in general and ISRN in particular, as well as an expansion of the ISRN-method to multi-variate data which is developed as part of this work to generate functional networks. An overview of the work flow for the generation of functional networks is shown in Fig. 4.

3.1. Recurrence networks

Recurrence networks are derived from recurrence plots [51]. The concept of recurrence in dynamical systems, prominent for example in recurrence quantification analysis, has developed into a well-studied field of research [52]. As an extensive amount of literature on this topic is already available, for example in [51,53], only a short introduction will be given in this section. Following the notation in [21], a recurrence plot is computed as follows. Measurements are taken from a dynamical system X at distinct times $t_i (i = 1, \dots, N^X)$. The dynamical system can be deterministic or stochastic [15]. By denoting $x_i = X(t_i)$, a time series $\{x_i\}_{i=1}^{N^X}$ is obtained. In the case of this study, the time series x_i represents the solution to a dynamical system represented by a second order differential equation. If the underlying system X is time-discrete, the time series data can be used directly. Time series data from

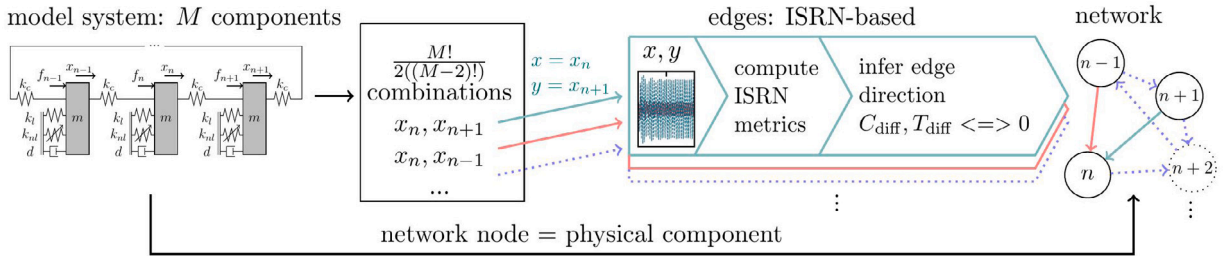

Fig. 4. Overview of the network generation process. Each of the M components of the model system becomes a node of the functional network. Here, each component is represented by a single Duffing oscillator. The direction of the edges between the nodes is determined via an iterative approach using ISRN measures. For every possible combination of two components (or, accordingly, nodes), time series measurements are obtained, an inter-system recurrence network is computed and the cross-clustering and transitivity measures are used to infer the direction of the edge between those two nodes. If $C_{\text{diff}} < -\mu, T_{\text{diff}} < -\mu$, the coupling direction is from X to Y, for $C_{\text{diff}} > \mu, T_{\text{diff}} > \mu$, it is Y to X, and for $-\mu < C_{\text{diff}} < \mu, -\mu < T_{\text{diff}} < \mu$ bi-directional coupling is defined. This process is repeated until each component has been compared with each other component, yielding $M!/(2(M-2)!)$ combinations in total. The resulting functional network is directed, but not weighted.

a time-continuous dynamical system has to be sampled with a finite frequency. A recurrence plot is defined as a matrix R^X with entries

$$R^X_{ij}(\varepsilon) = R^X(x_i, x_j|\varepsilon^X) = \Theta(\varepsilon^X - d(x_i, x_j)), \tag{3}$$

where $d(x_i, x_j) = \|x_i - x_j\|$ measures the supremum norm between two observations in phase space, Θ is the Heaviside function, and ε^X is a fixed distance measure. This threshold defines a fixed volume of the phase space, within which two observations are counted as recurrent. Alternatively, it is also possible to perform the analyses using the reconstructed phase space of the discrete time series obtained through delay embedding, at the cost of introducing two additional hyperparameters, namely the embedding dimension and the time delay. The recurrence network is obtained by interpreting the resulting recurrence matrix R^X as the adjacency matrix A^X of a network [47,49,50]. To exclude self-loops, the main diagonal of the adjacency matrix is set to zero with

$$A^X_{ij}(\varepsilon^X) = R^X_{ij}(\varepsilon^X) - \delta_{ij}, \quad \delta_{ij} = \begin{cases} 1, & i = j \\ 0, & i \neq j \end{cases}, \tag{4}$$

where δ_{ij} is the Kronecker delta. The resulting network has N^X nodes, which are connected if they lie within a fixed phase space volume ε^X of each other. Because the recurrence is defined through a fixed volume of the phase space, the network is called an ε-recurrence network. The resulting network is unweighted and undirected.

3.2. Inter-system recurrence networks

Inter-system recurrence networks [21] form an extension of the RN concept for bi-variate time series data. The following presentation follows the notation introduced in [21]. A description of the algorithm can also be found in [15]. To study the bi-variate case, a second dynamical system Y is introduced. The two dynamical systems X and Y should share the same physical units and phase space dimension to obtain physically meaningful results [15,21,51]. Applications of the inter-system recurrence theory to cases where systems do not share the same physical units or phase space are possible using specific transformation approaches [21]. However, results from these comparisons but should be interpreted carefully, as there is no mathematical foundation for the treatment of the conceptual problems that arise [21]. Analogously to the above description of a time series $\{x_i\}_{i=1}^{N^X}$ of a dynamical system X, the second dynamical system Y is measured at times $t_j (j = 1, \ldots, N^Y)$ to generate a second time series $\{y_j\}_{j=1}^{N^Y}$. The time series length and sampling frequency of the two time series $\{x_i\}_{i=1}^{N^X}$ and $\{y_j\}_{j=1}^{N^Y}$ do not need to be identical, as the method does not make use of time information directly, but leverages geometric properties of the system. Accordingly, both time series have to sample a sufficient part of the underlying attractor. For each of these time series, the corresponding adjacency matrices A^X and A^Y are obtained as defined in Eqs. (3) and (4), with fixed volumes ε^X and ε^Y of the phase space. Additionally, a cross-recurrence plot is computed as

$$CR^{XY}_{ij}(\varepsilon^{XY}) = \Theta(\varepsilon^{XY} - d(x_i, y_j)), \tag{5}$$

where $d(x_i, y_j) = \|x_i - y_j\|$ denotes the supremum norm between two observations of the two different time series. In contrast to the cross-recurrence plot, which requires two dynamical systems with identical phase space and physical units, but allows for arbitrary time series length and sampling points, an alternative method, exists. The joint recurrence plot requires identical time series length and sampling points, but allows for different phase space dimensions and physical units. The cross-recurrence matrix CR^{XY} defines the connectivity between two nodes of different networks [21]. As in an adjacency matrix, two nodes are connected if the respective entry in CR^{XY} equals one, and disconnected if the entry is zero. Due to the symmetry of the problem, the second cross-recurrence

matrix is the transpose of the first, $CR^{YX} = [CR^{XY}]^{\mathrm{T}}$. The ISRN is set up by combining the adjacency matrices A^X and A^Y derived from each time series with the cross-recurrence matrices CR^{XY} and CR^{YX} to an adjacency matrix

$$A^{\mathrm{ISRN}}(\boldsymbol{\varepsilon}) = \begin{bmatrix} A^X(\varepsilon^X) & CR^{XY}(\varepsilon^{XY}) \\ CR^{YX}(\varepsilon^{XY}) & A^Y(\varepsilon^Y) \end{bmatrix}, \tag{6}$$

where $\boldsymbol{\varepsilon} = [\varepsilon^X, \varepsilon^Y, \varepsilon^{XY}]$ comprises the fixed phase space thresholds for each individual computation. This inter-system recurrence network embodies a network with two sub-networks. The two adjacency matrices A^X and A^Y represent networks from the two individual systems, while the two cross-recurrence matrices CR^{XY} and CR^{YX} constitute the connections between the two networks.

The ISRN method requires a choice of the threshold parameters $\boldsymbol{\varepsilon}$. There are a number of studies on the determination of a suitable threshold parameter, for example in [46–48,54]. The threshold parameter ε determines the recurrence rate RR in the recurrence plot, and therefore the link density of the resulting recurrence network. For practical considerations, it is common to fix the recurrence rate instead of the threshold parameter in the context of recurrence networks [21]. Ideally, the recurrence rate is large enough such that most of the nodes in the resulting network are connected within one large component, but small enough to keep the overall connectivity small. For many systems, $RR < 0.05$ is a good choice [21]. To obtain an ISRN that represents two connected networks rather than one large network, there have to be more intra-system than inter-system connections. That is, the intra-system recurrence rates RR^X and RR^Y, defined by

$$RR = \frac{1}{N^2} \sum_i R_{ij} \tag{7}$$

have to be larger than the inter-system recurrence rate, which is given by

$$RR^{XY} = \frac{1}{N^X N^Y} \sum_{ij} CR_{ij}^{XY}, \tag{8}$$

as recommended in [21,46,48]. The inter-system recurrence rates RR^{XY} and RR^{YX} are kept identical, as the symmetry of these components is crucial to the proposed method, as described in the following section. Studies have shown that network measures depend on the choice of threshold parameter [47]. However, the method proposed in this work does not require exact quantities, but relies on the asymmetry of two network-based measures, which will be introduced in the next section. Therefore, it can be assumed that the exact choice of ε is not crucial for this method. In this work, the phase space thresholds in $\boldsymbol{\varepsilon}$ are chosen such that the recurrence rates are $RR^X = 0.03$, $RR^Y = 0.03$ and $RR^{XY} = 0.02$, based on the parameters given in [21]. The computation of the inter-system recurrence network and the related measures is performed using the pyunicorn package [55] in Python. Numerically expensive computations are performed in compiled C, C++, or FORTRAN code, rendering the computations relatively efficient. For example, computing a cross-clustering coefficient in Eq. (10) from a 2000×2000 adjacency matrix takes 0.17 s on a 12-core Intel Core i7 CPU with 2.6 GHz running Ubuntu 20.04.

3.3. Inference of functional interrelations

Two properties of the ISRN, namely the global cross-correlation coefficient C and the global cross-transitivity T, can be used to infer functional interrelations between two components X and Y [21]. A short definition and background of these two measures, based on the descriptions in [21,56], is given in this section. For more detailed information on general network properties, see [14,15]. The network measures are defined for a network $G = (V, E)$ with edges E and nodes $V = \{1, \ldots, N\}$. In the case of the ISRN, the network consists of the sub-networks V^X and V^Y. For the following description, consider a single node in sub-network V^X which is called v and two exemplary nodes of V^Y which are called p and q. The global cross-clustering coefficient C^{XY} describes the probability of a node $v \in V^X$ to have pairs of mutually connected neighbors in V^Y. It is calculated as the average over all local cross-clustering coefficients

$$C_v^{XY} = \frac{1}{k_v^{XY}(k_v^{XY} - 1)} \sum_{p,q \in V^Y} A_{vp}^{\mathrm{ISRN}} A_{pq}^{\mathrm{ISRN}} A_{qv}^{\mathrm{ISRN}}, \tag{9}$$

such that

$$C^{XY} = \langle C_v^{XY} \rangle_{v \in V^X}, \tag{10}$$

where $k_v^{XY} = \sum_{q \in V^Y} A_{vq}^{\mathrm{ISRN}}$ denotes the cross-degree. On the other hand, the cross-transitivity T^{XY} defines the probability that two nodes p, q in sub-network V^Y are connected if they are both connected to a node v in sub-network V^X. It is computed as

$$T^{XY} = \frac{\sum_{v \in V^X, p \neq q \in V^Y} A_{vp}^{\mathrm{ISRN}}}{A}{}^{\mathrm{ISRN}}_{pq} A_{qv}^{\mathrm{ISRN}} \sum_{v \in V^X, p \neq q \in V^Y} A_{vp}^{\mathrm{ISRN}} A_{vq}^{\mathrm{ISRN}}, \tag{11}$$

counting the number of "cross-triangles" over the number of "cross-triples". Both measures are not invariant under the permutation $X \leftrightarrow Y$, such that $C^{XY} \neq C^{YX}$ and $T^{XY} \neq T^{YX}$.

In our functional network, the direction of an edge between two nodes represents a functional relationship between the corresponding components. The basic idea of inferring a functional interrelation between two components using an ISRN is presented in [21]. In the case of uni-directional and attractive diffusive coupling from X to Y, the trajectory of Y is likely dragged towards the trajectory of X, increasing the probability of finding triangles $x - x - y$, which add to T^{YX} and C^{YX}, but not to T^{XY} and

Table 2
ISRN measures and related functional dependencies. A small threshold $\mu = 0.02$ is introduced to avoid wrong detection of coupling direction due to small asymmetries which may arise due to small system detuning or rounding.

Network measure	Functional dependency
$C_{\text{diff}} < -\mu, T_{\text{diff}} < -\mu$	X on Y
$C_{\text{diff}} > \mu, T_{\text{diff}} > \mu$	Y on X
$-\mu < C_{\text{diff}} < \mu, -\mu < T_{\text{diff}} < \mu$	Bi-directional or no dependency

C^{XY}. The opposite is true for the inverse dependency. Therefore, $T^{YX} > T^{XY}$ and $C^{YX} > C^{XY}$ is expected for a uni-directional interrelation $X \rightarrow Y$, and, accordingly, the opposite for the inverse dependency direction. For clarity, the differences are defined as $C_{\text{diff}} = C^{XY} - C^{YX}$ and $T_{\text{diff}} = T^{XY} - T^{YX}$ in this work, such that $C_{\text{diff}} > 0$ and $T_{\text{diff}} > 0$ implies a dependency of Y on X, and $C_{\text{diff}} < 0$ and $T_{\text{diff}} < 0$ implies dependency of X on Y. In the case when the two systems are not interrelated, the measures can be interpreted as arising randomly, such that $C_{\text{diff}} \approx 0$ and $T_{\text{diff}} \approx 0$. If the two systems share a symmetric bi-directional interrelation, an equal attraction between the two time series is expected, and thus $T^{YX} = T^{XY}$ and $C^{YX} = C^{XY}$, such that $C_{\text{diff}} = 0$ and $T_{\text{diff}} = 0$. Unfortunately, the method does not yield a clear distinction between the case of no interrelation and bi-directional dependency. For the purpose of this work, these ambiguous cases are always regarded as a bi-directional connection. The definition of $C_{\text{diff}} = T_{\text{diff}} = 0$ for no or bi-directional dependency is found to be too strict in the given use case, since even small detuning, for example in the natural frequencies of the two coupled systems, can lead to small asymmetries [15]. Therefore, a small threshold $\mu = 0.02$ is defined, such that $-\mu < C_{\text{diff}} < \mu, -\mu < T_{\text{diff}} < \mu$ define bi-directional or no interrelation, $C_{\text{diff}} < -\mu, T_{\text{diff}} < -\mu$ represents the X on Y- dependence case, and vice versa. A summary of the network measures and the corresponding functional dependencies can be found in Table 2.

This method of inferring the functional interrelation, or edge direction, between two dynamical systems from ISRN measures has a number of applications in literature, including the detection of coupling direction in a system of two coupled Rössler systems and paleoclimate data [21], and the study of oil-water flow states [25–27]. In this paper, the method is used in an iterative manner to generate a functional network from mechanical systems with more than two degrees of freedom. The procedure will be presented in the following section.

3.4. Generation of functional networks

Generating functional networks from a system of multiple connected components is the goal of this work. To achieve this, the method for inferring the functional interrelation between two components is applied in an iterative manner, as illustrated in Fig. 4.

The starting point in this study is a model system composed of five forced nonlinear Duffing oscillators, as introduced in Section 2. A single Duffing oscillator represents one component of the model system. Each of the M components of the dynamical system becomes a node in the functional network. To compute the connectivity of the nodes, the ISRN-based approach is taken. Every possible pairing of components is listed. By picking a pairing, for example, x_n and x_{n+1}, and defining the measured displacement time series from these components as $x_n = x$ and $x_{n+1} = y$, the ISRN analysis can be performed as described in Section 3.2. The edge direction between the two corresponding nodes n and $n+1$ is then determined according to the procedure in Section 3.3. This process is repeated until every combination of components (or nodes) has been analyzed. The resulting network has M nodes and $M!/(2((M-2)!))$ unweighted, directed edges. Per definition, there is an, either uni- or bi-directional, edge between each node and each other node.

In case of a 5-component or model system, the resulting network has five nodes, and can be described by an adjacency matrix $A^{\text{ISRN}} \in \mathbb{R}^{5\times5}$. An exemplary network is shown on the left in Fig. 5, and the corresponding adjacency matrix A^{ISRN} is given in Eq. (12). To get a clearer image of the resulting network, a network condensation is performed in a last step. Bidirectionally connected nodes that share the same in- and out-edges, such as the nodes “3” and “4” in the aforementioned graph, are combined into a single node “34”. Once all nodes are combined in this way, the edges between them are derived from the edges in the original graphs. The resulting condensed network has a number of edges $E \leq N$. For the exemplary network, the condensed version is shown on the right-hand side in Fig. 5, and the respective adjacency matrix $A^{\text{cond}} \in \mathbb{R}^{5\times5}$ is presented in Eq. (12). This visualization scheme is related to community detection algorithms [57], and allows for a better overview over the connections and symmetries within the graph.

To summarize, the networks in Fig. 5 are described by the adjacency matrices A^{ISRN} and A^{cond} as

$$A^{\text{ISRN}} = \begin{bmatrix} 0 & 1 & 1 & 1 & 1 \\ 1 & 0 & 1 & 1 & 1 \\ 0 & 0 & 0 & 1 & 1 \\ 0 & 0 & 1 & 0 & 1 \\ 0 & 0 & 0 & 0 & 0 \end{bmatrix} \rightarrow A^{\text{cond}} = \begin{bmatrix} 0 & 1 & 1 \\ 0 & 0 & 1 \\ 0 & 0 & 0 \end{bmatrix}, \tag{12}$$

where the nodes in the second matrix A^{cond} are ordered by “12”–“34”–“5”. Each of the nodes in the condensed network represents a “functional cluster”, the nodes within exhibit similar dynamical behavior. For example, the node “12” combines nodes “1” and “2” together, indicating a dynamical similarity between the two. Links, or edges, between these functional clusters represent a functional

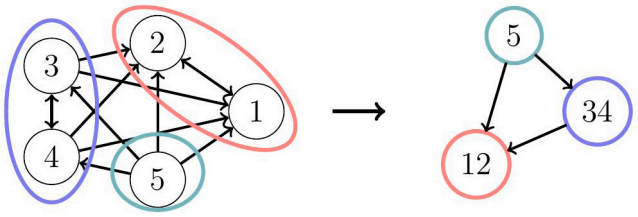

Fig. 5. Condensation of a five-dimensional network to a lower dimensional one. Bidirectionally connected nodes with identical in- and out-edges are combined into one node, allowing for a better overview of the graph structure. The corresponding adjacency matrices A^{ISRN} and A^{cond} are given in Eq. (12).

relationship between these components. Each non-zero entry in the adjacency matrix defines an edge, such that $A[i, j]$ describes an edge from node i to node j. Note that the diagonal of the adjacency matrix is always zero in this work, since self-loops, or links from one node to itself, are not allowed. Both the original and the condensed adjacency matrix are typically non-symmetric in this study, as the networks are directed. The description of the system dynamics as a functional network allows for studying a number of node–related as well as global network measures.

For example, the network size is defined by the number of nodes in the network, which is given by N for the original and by $E \leq N$ for the condensed network. Node properties can be studied in terms of in- and out-degree. The former, defined as

$$k_{\mathrm{in},p} = \sum_{q=1}^{E} A_{qp}^{\mathrm{cond}} \tag{13}$$

for the pth node, describes the number of in-links to a specific node. The out-degree represents the number of out-links from a node, and is given by

$$k_{\mathrm{out},p} = \sum_{q=1}^{E} A_{pq}^{\mathrm{cond}} \tag{14}$$

for the pth node. Each degree-measure can be summarized to a global network characteristic, the average in- or out-degree, which is defined as

$$k_{\mathrm{avg}} = 1/E \sum_{p=1}^{E} k_p, \tag{15}$$

where k can be k_{in} or k_{out}. A large number of additional network measures, such as clustering, efficiency, or average shortest path length, exist [15]. An in-depth study of these additional measures on the functional network is left for future work, as larger systems will likely make these analyses especially interesting.

4. Results

This work seeks to complement the geometry-based view of a mechanical dynamical system as a set of components and their geometric connections by a functional perspective. In our functional networks, each node represents a mechanical component, and an edge between two components indicates the functional connection between them. We thus hope to uncover a functional structure for the underlying dynamics, revealing some more insight into the inner workings of the system. Such a functional structure could yield insight into how the mechanical components interact with each other, and which of the components dominate the systems dynamics. To this end, the iterative network-based approach described in Section 3.4 is applied to time series data obtained from the model system of five cyclically coupled Duffing oscillators of Section 2. Two studies are performed: In the first study, functional networks are generated from each of the dynamical states presented in Fig. 2. Two versions of the study are performed, one using the entire time series and one discarding the transients, such that only the steady-state dynamics are considered. Thus, networks from both transient and steady-state dynamics are obtained. The second study focuses on networks from transient dynamics. The first front-like dynamics (panel (g) in Fig. 3), where an initial disturbance is propagated through the system, is investigated in more detail. To do so, consecutive smaller samples are taken from the time series, and functional networks are computed for each sample, unveiling the evolution of the functional dependencies over time. The results are shown in the following.

Fig. 6 shows the resulting networks for each of the system dynamics presented in Fig. 2. For every dynamical state, three different networks are shown. On the left-hand side, the functional network inferred from the entire time series is shown in black, and the network obtained when discarding the first 1500 time steps as transients in blue in the middle. On the right, the condensed networks obtained following the procedure described in Section 3.4 are shown in red. Where the first two networks are not identical, two condensed networks are shown.

Per definition of the method, there is an edge between each node and each other node in all networks. The functional networks differ only in direction of the edges, which can be uni- or bidirectional. In contrast, the reduced networks vary in both size E and link direction, as described by the node in- and out-degrees $\boldsymbol{k}_{\mathrm{in}}$ and $\boldsymbol{k}_{\mathrm{out}}$. Table 3 summarizes the results in terms of network measures of the condensed network.

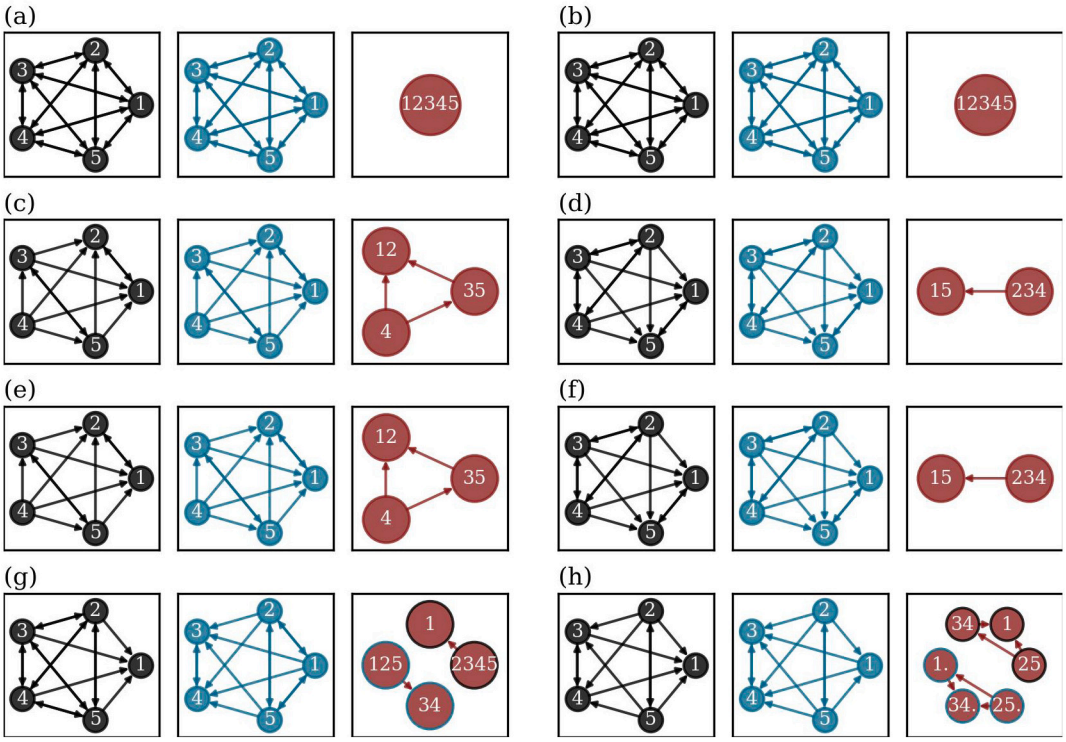

Fig. 6. Functional networks from systems of five Duffing oscillators with nearest-neighbor coupling operating in different dynamical states. For each state, the functional network generated from the entire time series is shown in black on the left, the network obtained when discarding the first 1500 time steps of each time series as transients in blue in the middle, and the smaller networks, where similar nodes are combined for clarity, as shown in red in the right panel. Images correspond to the dynamics shown in Fig. 3: Uniform oscillation with (a) low and (b) high amplitude, localized harmonic vibrations of (c) one and (d) three oscillators, localized higher-periodic vibrations of (e) one and (f) three oscillators, front like dynamics (g) one and (h) two. For the last two cases (g) and (h), where the networks with and without transients are not identical, two condensed networks as shown. The edge color of the nodes in the reduced network shows which larger network it relates to. (For interpretation of the references to color in this figure legend, the reader is referred to the web version of this article.)

Table 3
Network measures: analysis of the condensed functional networks.

Case	Size E	Node list	In-degrees $\boldsymbol{k}_{\text{in}}$	Out-degrees $\boldsymbol{k}_{\text{out}}$
(a)	1	["12345"]	–	–
(b)	1	["12345"]	–	–
(c)	3	["12", "35", "4"]	[2, 1, 0]	[0, 1, 2]
(d)	2	["15", "234"]	[1, 0]	[0, 1]
(e)	3	["12", "35", "4"]	[2, 1, 0]	[0, 1, 2]
(f)	2	["15", "234"]	[1, 0]	[0, 1]
(g.1)	2	["1", "2345"]	[1, 0]	[0, 1]
(g.2)	2	["125", "34"]	[0, 1]	[1, 0]
(h.1)	3	["1", "25", "34"]	[2, 0, 1]	[0, 2, 1]
(h.2)	3	["1", "25", "34"]	[1, 0, 2]	[1, 2, 0]

The top two cases (a) and (b) show functional networks generated from uniform oscillation with low and high amplitude, respectively. Both functional networks are fully connected with all bi-directional edges, resulting in a functional network of size $E_{\text{a,b}} = 1$. The corresponding condensed network has a single node "12345", since all nodes with bi-directional links that share the same in- and out-edges get combined into one. There is no difference between the networks obtained with and without transients.

The system with a localized vibration of one oscillator at high amplitude in (c) yields a less homogeneous functional network. The functional networks generated from the full and the truncated time series are the same. Most of the edges become uni-directional, except for bi-directional edges between the nodes "1" and "2", and "3" and "5", which are integrated into functional clusters. Accordingly, the size of the condensed network is $E_{\text{c}} = 3$, with nodes ["12", "35", "4"]. The node list captures the symmetry within the system: node "4" corresponds to the component that vibrates at high amplitude, and the remaining nodes are combined in accordance with their distance to this component. The lists of in- and out-degrees encodes a functional hierarchy within the network. The node "4", the node with the lowest in- and highest out-degree, appears as leading node with edges to "12" and "35". An additional edge from "35" to "12" can be observed, making node "12" the one with the highest in- and lowest out-degree.

The localized vibration with three masses at high amplitudes (d) results in a slightly different functional network. Additional bi-directional edges between "2" and "4", and "3" and "4" produce a reduced network with two nodes and size $E_{\mathrm{d}} = 2$. Two functional clusters represent the masses at high amplitude "234", and the masses at low amplitude "15"once again capturing the symmetry within the system. In accordance with previous results, the edge between the two points from the higher to the lower amplitude, that is from "234" to "15", as can be observed from the respective list of in- and out-degrees in Table 3.

The cases with higher-periodic motion (e) and (f) yield the same results as their counterparts in localized harmonic motion, (c) and (d). For all four cases, the inclusion or omission of the transients does not appear to have an impact on the resulting functional network.

The bottom panels (g) and (h) show the two different functional networks generated from the front-like dynamics. For all previous cases (a)–(f), dropping the transients had no impact on the result. For front 1 and front 2, the functional networks from the full time series and from the truncated time series differ. The color of the node edges indicates which time series they relate to. In Table 3, (g.1) refers to the black-edged network from the full time series, while (g.2) refers to the blue-edges network from the truncated time series. The same notation applies for the case (h). In the first case, the number and location of the bi-directional edges changes. The result are two different condensed networks with two nodes each. The functional network obtained from the full time series is described by the node list ["1", "2345"], and in-degrees [1, 0], indicating a link from node "2345" to node "1". The network from the truncated time series has two different nodes "125" and "34", with an edge from "125" to "34". Both the functional clustering of the nodes as well as the dominant link directionality change over time. In the case of the second front-like dynamics, the bi-directional edges do not change, such that the combination of nodes to functional clusters remains unchanged. The links between the nodes differ, as the different node in- and out-degrees show. While both networks share edges from "25" to "1" and "34", the network from the full time series has an edge from "34" to "1", which inverts its direction in the network from the truncated time series. This observation motivates a detailed study of the transient dynamics in the following.

In the second study, the analysis is performed by windowing the time series into 5 s samples, from each of which a functional network is generated. The front-like dynamics in Fig. 2(g) are generated by excitation with a frequency $\Omega = 1.873$ rad s^{-1} at the border of the bi-stability region. Only the first mass is displaced initially. Due to the particular excitation frequency at the border of the bi-stability region, the high-amplitude state propagates through the system, until all masses oscillate in synchrony at the high amplitude.

Fig. 7 shows exemplary functional networks in full and condensed form as well as the corresponding dynamics for exemplary samples during the synchronization process. It can be observed that the condensed network size $E_{\mathrm{g,t=0:75}} = 3$ is constant most of the time, but drops to $E_{\mathrm{g,t=0:125}} = 1$ as the model components synchronize. The partition into functional clusters "1", "25" and "34", which remains constant through the process, until all nodes merge into one functional cluster "12345" at $t = 125$. This consistent division into three parts stands in contrast to the two different partitions into two parts obtained when using a longer section of the time series. Similarly to the case with a localized mass, the network encodes the symmetry of the dynamics. Node "1" corresponds to the mass that is initially displaced, while the remaining components are divided into nodes according to their proximity to the single node. The direction of the links between the nodes changes over time, and with it the in- and out-degrees of the nodes. In Fig. 7, black arrows indicate edge directions where both measures agree, as before. In some cases, the two network measures C_{diff} or T_{diff} do not agree on the direction. The edge directions according to C_{diff} are shown in orange, the ones according to T_{diff} in blue. Only the out-degrees of the nodes will be listed in the following, counting solely the links that are indicated by both measures.

The first image for $0 < t < 5$ on the left depicts a functional network analogous to the one for the case of a single mass oscillating at high amplitude in panel (c) in Fig. 6. In the dynamics of the sample, the first mass oscillates not only with higher amplitude, but also with higher frequency, and starts pulling the other masses towards its dynamics. The edge direction in the network, encoded in the list of out-degrees $\boldsymbol{k}_{\mathrm{out,t=0}} = [2, 1, 0]$, can be interpreted as representing this fact. At $17.5 < t < 22.5$, all masses oscillate with similar, higher amplitude, but heterogeneous frequencies. The out-degrees change to $\boldsymbol{k}_{\mathrm{out,t=17.5}} = [2, 0, 0]$, indicating that the two edges pointing away from node "1" remain the same. For the edge between "25" and "34", the two network measures do not agree on the link direction. This discrepancy can be interpreted as an indicator for the onset of change: In the next, overlapping sample $20 < t < 25$, the affected edge "25"–"34" has changed direction, resulting in new out-degrees $\boldsymbol{k}_{\mathrm{out,t=20}} = [1, 0, 2]$. The "1" to "25" link is still unchanged, while the "1" to "34" link inverts. According to the measure C_{diff}, there is a bi-directional link between "1" and "34", probably as a result of the transition in link direction. In the dynamics of the corresponding sample, the third and fourth oscillator vibrate with the highest frequency, the other masses following with a phase lag. Oscillator 2 and 5 appear to have a slightly slower frequency than the first oscillator. In the fourth sample, the masses have almost synchronized at the high amplitude, but masses 3 and 4 are, in terms of their phase, visibly ahead of the other masses. This phenomenon is visible in the corresponding network, where the "34" node now "pulls" the other nodes, and in the out-degrees list, which now reads $\boldsymbol{k}_{\mathrm{out,t=47.5}} = [0, 1, 2]$. All edges have changed direction compared to the initial functional network on the left, inverting the functional hierarchy of model components. The fifth panel shows a transition phase, where the two networks measures only agree on a minority of link directions indicated by $\boldsymbol{k}_{\mathrm{out,t=75}} = [1, 1, 0]$. This phenomenon seems to be an expression of the transition process, as the system moves to full synchronization in the right and last panel. As expected from previous results, the corresponding functional network for uniform motion is a fully connected network with all-bidirectional edges. Accordingly, the node out-degrees are given by $\boldsymbol{k}_{\mathrm{out,t=125}} = [2, 2, 2]$. In accordance with previous explanations, the reduced network would be a single "12345"-node as shown in panels (a) and (b) of Fig. 6, but to stay consistent with the remainder of this figure, the three-wise split has been kept.

In summary, the condensed networks shown in Fig. 6, which are obtained from different global system states, encode dynamics-based, functional dependencies within the system. Functional clusters, formed by merging similar nodes of the functional network together, correspond to components with similar dynamics. Links between these clusters represent functional dependencies within

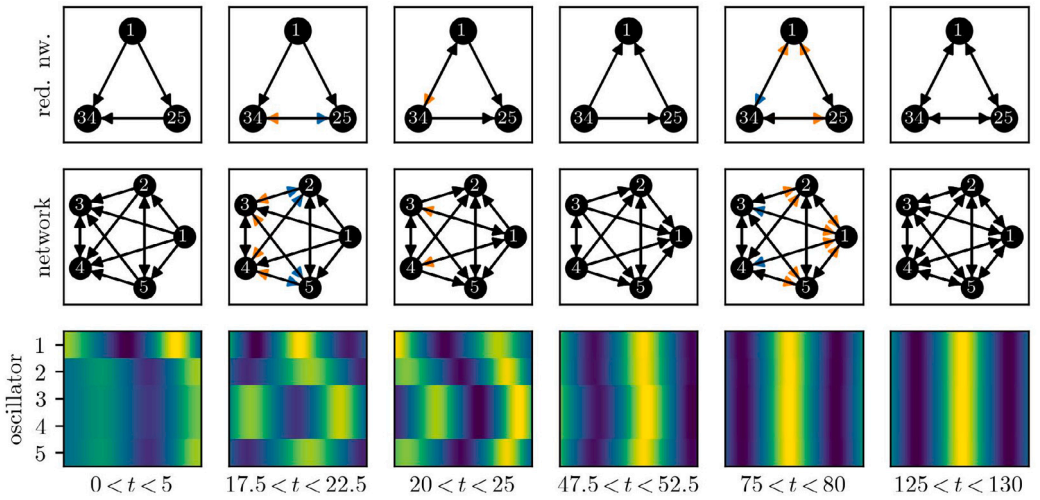

Fig. 7. Functional networks generated from time series samples of 5 s length illustrate the synchronization mechanism. The model system consists of five Duffing oscillators with nearest-neighbor coupling, excitation at frequency $\Omega = 1.873$ rad s^{-1} at the border of the bi-stability region and initial displacement of a single mass ("1"). The networks are generated as before. Black arrows indicate edges where the two metrics C_{diff} or T_{diff} agree on the direction. Where the measures do not agree, the coupling directions according to C_{diff} are shown in orange, the ones according to T_{diff} in blue. (For interpretation of the references to color in this figure legend, the reader is referred to the web version of this article.)

the system. The observation that including the transients in the data does not affect the resulting functional networks in cases (a)–(f) is likely due to the fact that these transients represent only a relatively short section of the time series data. The results indicate that the network analysis filters out dominant functional relationships over the given time period, and that the comparatively short-lived transients live on a time scale that is too small to be resolved. The data underlying cases (g) and (h) is dominated by transient motion on a larger time scale, which is captured by the analysis of even these relatively long time series sections. The second part of the analysis, which focuses on small samples of the time series in (g) at a time, resolves the functional structure on a smaller time scale. This change in the time resolution of the analysis yields different functional clusters and functional dependencies within the system, depending on the time scale to be resolved.

5. Discussion

This study uses ISRN metrics to generate functional networks to study the complex dynamics of a mechanical model system composed of nonlinear Duffing oscillators. Within the functional network, each node represents a mechanical component, and the edges correspond to functional dependencies between the respective components. Per definition of the iterative process, the resulting networks have an edge between each node, the direction of which is identified from the network metrics cross-clustering coefficient and cross-transitivity. This approach provides an alternative perspective onto multi-dimensional nonlinear systems, which focuses on function-based interrelations rather than geometrical proximity. As this study presents a novel approach at an early stage, there are still numerous compelling avenues for exploration and interesting paths to pursue.

The resulting reduced network shows the diversity of motion within a given system: In the case of uniform oscillation, there is only one distinct system state. In the case of localized vibration with one mass, there are three different types of motion: The oscillator with initial displacement is clearly in a different state than the other oscillators. The remaining oscillators are split into groups according to their proximity to the perturbed mass, based on the different time evolution in their respective transient motion. For the localized vibration with three masses, there are only two nodes in the reduced network, corresponding to the two distinct states in the time series. The functional networks make no distinction of the specific dynamics of a single oscillator, there is no difference in the results for a single-period localized vibration or a higher-periodic localized vibration. This finding is closely related to studies concerning the detection of network size from sparse measurements [58,59], or data-based reduced order modeling [60,61] and could be a starting point for further investigation. A novel reduced-order modeling approach could entail clustering degrees of freedom according to their dynamical similarity instead of the geometrical connection, as for example in the combination "35" in network (c) in Fig. 6. Perhaps the detected network size could also be a proxy for the complexity of the underlying dynamics, indicating the number of active states. The identified number of system states yields useful information on how many sensors are necessary to resolve the dynamics of the full system, as well as where to place them. For example, from network (a) in Fig. 6, it can be assumed that a single sensor placed on any of the components is sufficient to get complete measurement of the system dynamics, while for network (c), three sensors are required. This assumption is of course limited to cases such as the one presented here, where number and combination of nodes in the condensed network does not change over time.

Additionally, the presented method can track the time evolution of inter-dependencies within a system, because only a short time series is necessary for the setup of the network [21]. By exploiting this time-evolving network, the interplay of oscillators

during the synchronization process can be made visible. In the case at hand, the mechanism is not simply defined by one mass pulling the others along, but a more intricate process during which the hierarchy of oscillators changes, which ultimately leads to all masses oscillating with the high amplitude. Based on these observations, this method could represent a possibility for developing early warning strategies against dynamical transitions, which might be applied in structural health monitoring. Additionally, this approach could also help understanding the dependencies within a machine and thus form the basis for interfering with the process to avoid catastrophic events. Here, it could be possible to prevent the initial system disturbance from spreading over the entire system by simply disrupting the process or changing one of the intermediate components. For example, further studies might help to identify joints which are especially relevant for the system dynamics, such that modeling and design efforts can be focused accordingly. A possible extension to the proposed method is the distinction between direct and indirect coupling [33], similar to methods proposed in [62–64].

The results presented in this work are obtained from time series data with no added noise. For future application to real-world data, which is generally noise contaminated, the effects of noise on the functional network will be taken into account. The effects of noise on statistical features of the recurrence plot and respective analysis have been studied in detail for example in [65]. While recurrence-based analyses are generally very susceptible to noise, reliable results can still be obtained for moderate noise levels (below 20% of the standard deviation of the underlying time series), when the threshold parameter ε is chosen appropriately [15,65]. Even though detailed studies on the effect of noise on this specific recurrence-based method are still required, we are confident that our method would work for low to moderate noise levels.

6. Conclusion

In this work, an approach for inferring functional networks from data obtained from mechanical model systems is introduced, which hopes to complement conventional tools for the analysis of large multi-component systems. By assigning each physical component one network node, and connecting the nodes based on inter-system network measures cross-clustering coefficient and cross-transitivity, the functional network provides a new, function-based perspective on the dynamics of complex mechanical systems. The method is applied to a system of five Duffing oscillators with nearest-neighbor coupling operating in different dynamical states such as uniform oscillation, localized vibrations, and fronts. For each of these, a functional network is computed. By concatenating "equivalent" nodes together, a condensed network is obtained, which allows for a number of different network-based analyses. The size of the condensed network, given by the number of nodes, corresponds to the number of different dynamical states within a system. Each of the nodes within the condensed network form a functional cluster of dynamically similar components, and capture the symmetry within the system dynamics. Links between the clusters represent functional dependencies within the dynamical system. These functional relationships encode the global system state. These analyses could provide a basis for better sensor placement, insight into dynamic symmetries and thus a more efficient system analysis. The study of transient motion, or the propagation of a disturbance through the system, is made possible with a sliding-window technique. By analyzing small samples of the time series data over the course of time, the propagation of a disturbance through the dynamical system is studied. The corresponding functional networks facilitate the analysis of the transient dynamics and the interplay of the system components over time. We hope that this analysis of transient dynamics using network methods will pave the way for further studies, improved sensor placement, early warning methods, and counter-measures against potentially harmful vibrations.

CRediT authorship contribution statement

Charlotte Geier: Writing – review & editing, Writing – original draft, Visualization, Software, Methodology, Investigation, Formal analysis, Conceptualization. **Merten Stender:** Writing – review & editing, Funding acquisition. **Norbert Hoffmann:** Writing – review & editing, Supervision, Funding acquisition, Conceptualization.

Declaration of competing interest

The authors declare that they have no known competing financial interests or personal relationships that could have appeared to influence the work reported in this paper.

Data availability

Data will be made available on request.

Acknowledgments

C.G. is thankful to the DFG (German Research Foundation) for support through project number 510246309. The authors would like to thank Mathies Wedler for proof reading the article.

Appendix. Initial conditions for numerical data

See Table A.1.

Table A.1
Initial conditions for the numerical data generation presented in Section 2. The data resulting data is depicted in Fig. 3.

Case	Initial condition
(a)	$\boldsymbol{x}_{0,a} = [0, 0, 0, 0, 0, 0, 0, 0, 0, 0]$
(b)	$\boldsymbol{x}_{0,b} = [1, 1, 1, 1, 1, 0, 0, 0, 0, 0]$
(c)	$\boldsymbol{x}_{0,c} = [0, 0, 0, 1, 0, 0, 0, 0, 0, 0]$
(d)	$\boldsymbol{x}_{0,d} = [0, 1, 1, 1, 0, 0, 0, 0, 0, 0]$
(e)	$\boldsymbol{x}_{0,e} = [0, 0, 0, 0, 0, 0, 0, 0, 0, 0]$
(f)	$\boldsymbol{x}_{0,f} = [0, 0, 0, 0, 0, 0, 0, 0, 0, 0]$
(g)	$\boldsymbol{x}_{0,g} = [1, 0, 0, 0, 0, 0, 0, 0, 0, 0]$
(h)	$\boldsymbol{x}_{0,h} = [0, 1, 1, 1, 1, 0, 0, 0, 0, 0]$

References

[1] M. Stender, S. Oberst, M. Tiedemann, N. Hoffmann, Complex machine dynamics: systematic recurrence quantification analysis of disk brake vibration data, Nonlinear Dynam. 97 (4) (2019) 2483–2497, http://dx.doi.org/10.1007/s11071-019-05143-x.

[2] A. Papangelo, F. Fontanela, A. Grolet, M. Ciavarella, N. Hoffmann, Multistability and localization in forced cyclic symmetric structures modelled by weakly-coupled duffing oscillators, J. Sound Vib. 440 (1859) (2019) 202–211, http://dx.doi.org/10.1016/j.jsv.2018.10.028.

[3] M.R. Brake, The Mechanics of Jointed Structures, first ed., Springer International Publishing AG, Cham, 2018, http://dx.doi.org/10.1007/978-3-319-56818-8.

[4] S. Kruse, M. Tiedemann, B. Zeumer, P. Reuss, H. Hetzler, N. Hoffmann, The influence of joints on friction induced vibration in brake squeal, J. Sound Vib. 340 (2015) 239–252, http://dx.doi.org/10.1016/j.jsv.2014.11.016.

[5] A.T. Mathis, N.N. Balaji, R.J. Kuether, A.R. Brink, M.R.W. Brake, D.D. Quinn, A review of damping models for structures with mechanical Joints1, Appl. Mech. Rev. 72 (4) (2020) http://dx.doi.org/10.1115/1.4047707.

[6] M.S. Gadala, M.A. Dokainish, G.A. Oravas, Formulation methods of geometric and material nonlinearity problems, Internat. J. Numer. Methods Engrg. 20 (5) (1984) 887–914, http://dx.doi.org/10.1002/nme.1620200508.

[7] F. Walport, L. Gardner, E. Real, I. Arrayago, D.A. Nethercot, Effects of material nonlinearity on the global analysis and stability of stainless steel frames, J. Constr. Steel Res. 152 (2019) 173–182, http://dx.doi.org/10.1016/j.jcsr.2018.04.019.

[8] G. de Sitter, C. Devriendt, P. Guillaume, E. Pruyt, Operational transfer path analysis, Mech. Syst. Signal Process. 24 (2) (2010) 416–431, http://dx.doi.org/10.1016/j.ymssp.2009.07.011.

[9] D.J. Ewins, Modal Testing: Theory and Practice, second ed., Research Studies Press, Baldock, England, 2000.

[10] D. de Klerk, A. Ossipov, Operational transfer path analysis: Theory, guidelines and tire noise application, Mech. Syst. Signal Process. 24 (7) (2010) 1950–1962, http://dx.doi.org/10.1016/j.ymssp.2010.05.009.

[11] R. Albert, A.-L. Barabási, Statistical mechanics of complex networks, Rev. Mod. Phys. 74 (1) (2002) 47–97, http://dx.doi.org/10.1103/RevModPhys.74.47.

[12] P.B. Jain, T.T. Nguyen, R.C. Budzinski, J. Mináč, L.E. Muller, Synchronization patterns and stability of solutions in multiplex networks of nonlinear oscillators, 2023, http://dx.doi.org/10.48550/arXiv.2306.06532, arXiv preprint.

[13] L. Lacasa, R. Toral, Description of stochastic and chaotic series using visibility graphs, Phys. Rev. E 82 (3) (2010) 1078, http://dx.doi.org/10.1103/PhysRevE.82.036120.

[14] M. Newman, Networks, second ed., Oxford University Press, Oxford, 2018, http://dx.doi.org/10.1093/oso/9780198805090.001.00010.

[15] Y. Zou, R.V. Donner, N. Marwan, J.F. Donges, J. Kurths, Complex network approaches to nonlinear time series analysis, Phys. Rep. 787 (2019) 1–97, http://dx.doi.org/10.1016/j.physrep.2018.10.005.

[16] L. Astolfi, F. Cincotti, D. Mattia, M.G. Marciani, L.A. Baccala, F. de Vico Fallani, S. Salinari, M. Ursino, M. Zavaglia, L. Ding, J.C. Edgar, G.A. Miller, B. He, F. Babiloni, Comparison of different cortical connectivity estimators for high-resolution EEG recordings, Hum. Brain Mapp. 28 (2) (2007) 143–157, http://dx.doi.org/10.1002/hbm.20263.

[17] X. Zhang, S. Hallerberg, M. Matthiae, D. Witthaut, M. Timme, Fluctuation-induced distributed resonances in oscillatory networks, Science 5 (7) (2019) eaav1027, http://dx.doi.org/10.1126/sciadv.aav1027.

[18] X. Zhang, M. Timme, Fluctuation response patterns of network dynamics – An introduction, Eur. J. Appl. Math. 34 (3) (2023) 429–466, http://dx.doi.org/10.1017/S0956792522000201.

[19] M. McCullough, K. Sakellariou, T. Stemler, M. Small, Regenerating time series from ordinal networks, Chaos 27 (3) (2017) 035814, http://dx.doi.org/10.1063/1.4978743.

[20] J. Zhang, J. Sun, X. Luo, K. Zhang, T. Nakamura, M. Small, Characterizing pseudoperiodic time series through the complex network approach, Phys. D 237 (22) (2008) 2856–2865, http://dx.doi.org/10.1016/j.physd.2008.05.008.

[21] J.H. Feldhoff, R.V. Donner, J.F. Donges, N. Marwan, J. Kurths, Geometric detection of coupling directions by means of inter-system recurrence networks, Phys. Lett. A 376 (46) (2012) 3504–3513, http://dx.doi.org/10.1016/j.physleta.2012.10.008.

[22] T. Tanizawa, T. Nakamura, F. Taya, M. Small, Constructing directed networks from multivariate time series using linear modelling technique, Phys. A 512 (2018) 437–455, http://dx.doi.org/10.1016/j.physa.2018.08.137.

[23] M.A. Kramer, U.T. Eden, S.S. Cash, E.D. Kolaczyk, Network inference - with confidence - from multivariate time series, Phys. Rev. E 79 (6) (2009) 528, http://dx.doi.org/10.1103/PhysRevE.79.061916.

[24] A. Gozolchiani, K. Yamasaki, O. Gazit, S. Havlin, Pattern of climate network blinking links follows El Niño events, Europhys. Lett. 83 (2) (2008) 28005, http://dx.doi.org/10.1209/0295-5075/83/28005.

[25] Z.-K. Gao, X.-W. Zhang, N.-D. Jin, N. Marwan, J. Kurths, Multivariate recurrence network analysis for characterizing horizontal oil-water two-phase flow, Phys. Rev. E 88 (3) (2013) 032910, http://dx.doi.org/10.1103/PhysRevE.88.032910.

[26] Z.-K. Gao, Y.-X. Yang, Q. Cai, S.-S. Zhang, N.-D. Jin, Multivariate weighted recurrence network inference for uncovering oil-water transitional flow behavior in a vertical pipe, Chaos 26 (6) (2016) 063117, http://dx.doi.org/10.1063/1.4954271.

[27] Z.-K. Gao, Y.-X. Yang, L.-S. Zhai, W.-D. Dang, J.-L. Yu, N.-D. Jin, Multivariate multiscale complex network analysis of vertical upward oil-water two-phase flow in a small diameter pipe, Sci. Rep. UK 6 (2016) 20052, http://dx.doi.org/10.1038/srep20052.

[28] L. Lacasa, V. Nicosia, V. Latora, Network structure of multivariate time series, Sci. Rep. UK 5 (2015) 15508, http://dx.doi.org/10.1038/srep15508.

[29] D. Eroglu, N. Marwan, M. Stebich, J. Kurths, Multiplex recurrence networks, Phys. Rev. E 97 (1) (2018) 1, http://dx.doi.org/10.1103/PhysRevE.97.012312.

[30] M.C. Romano, M. Thiel, J. Kurths, I.Z. Kiss, J.L. Hudson, Detection of synchronization for non-phase-coherent and non-stationary data, Europhys. Lett. 71 (3) (2005) 466–472, http://dx.doi.org/10.1209/epl/i2005-10095-1.

[31] J.H. Feldhoff, R.V. Donner, J.F. Donges, N. Marwan, J. Kurths, Geometric signature of complex synchronisation scenarios, Europhys. Lett. 102 (3) (2013) 30007, http://dx.doi.org/10.1209/0295-5075/102/30007.

[32] M. Jachan, K. Henschel, J. Nawrath, A. Schad, J. Timmer, B. Schelter, Inferring direct directed-information flow from multivariate nonlinear time series, Phys. Rev. E 80 (1 Pt 1) (2009) 011138, http://dx.doi.org/10.1103/PhysRevE.80.011138.

[33] J. Zhang, J. Zhou, M. Tang, H. Guo, M. Small, Y. Zou, Constructing ordinal partition transition networks from multivariate time series, Sci. Rep. UK 7 (1) (2017) 7795, http://dx.doi.org/10.1038/s41598-017-08245-x.

[34] G. Terrones, D.W. McLaughlin, E.A. Overman, A.J. Pearlstein, Stability and bifurcation of spatially coherent solutions of the damped-driven NLS equation, SIAM J. Appl. Math. 50 (3) (1990) 791–818, http://dx.doi.org/10.1137/0150046.

[35] D.J. Kaup, A.C. Newell, Theory of nonlinear oscillating dipolar excitations in one-dimensional condensates, Phys. Rev. B 18 (10) (1978) 5162–5167, http://dx.doi.org/10.1103/PhysRevB.18.5162.

[36] F. Fontanela, Solitons in Cyclic and Symmetric Structures (Ph.D. thesis), Imerial College London, 2018.

[37] T. Hoffmann, L. Panning-von Scheidt, J. Wallaschek, Analysis of contacts in friction damped turbine blades using dimensionless numbers, J. Eng. Gas Turb. Power 141 (12) (2019) http://dx.doi.org/10.1115/1.4044481.

[38] T. Hoffmann, L. Panning-von Scheidt, J. Wallaschek, Measured and simulated forced response of a rotating turbine disk with asymmetric and cylindrical underplatform dampers, J. Eng. Gas Turb. Power 142 (5) (2020) http://dx.doi.org/10.1115/1.4045337.

[39] I. Kovacic, M.J. Brennan, The Duffing Equation: Nonlinear Oscillators and Their Phenomena, first ed., John Wiley & Sons, Ltd., Chichester West Sussex U.K. and Hoboken N.J., 2011, http://dx.doi.org/10.1002/97804709778590.

[40] Y. Ueda, Survey of regular and chaotic phenomena in the forced duffing oscillator, Chaos Solitons Fractals 1 (3) (1991) 199–231, http://dx.doi.org/10.1016/0960-0779(91)90032-5.

[41] M. Stender, N. Hoffmann, bSTAB: an open-source software for computing the basin stability of multi-stable dynamical systems, Nonlinear Dynam. 107 (2) (2022) 1451–1468, http://dx.doi.org/10.1007/s11071-021-06786-5.

[42] Y.S. Kivshar, M. Peyrard, Modulational instabilities in discrete lattices, Phys. Rev. A 46 (6) (1992) 3198–3205, http://dx.doi.org/10.1103/PhysRevA.46.3198.

[43] A. Papangelo, N. Hoffmann, A. Grolet, M. Stender, M. Ciavarella, Multiple spatially localized dynamical states in friction-excited oscillator chains, J. Sound Vib. 417 (2018) 56–64, http://dx.doi.org/10.1016/j.jsv.2017.11.056.

[44] P. Virtanen, R. Gommers, T.E. Oliphant, M. Haberland, T. Reddy, D. Cournapeau, E. Burovski, P. Peterson, W. Weckesser, J. Bright, S.J. van der Walt, M. Brett, J. Wilson, K.J. Millman, N. Mayorov, A.R.J. Nelson, E. Jones, R. Kern, E. Larson, C.J. Carey, İ. Polat, Y. Feng, E.W. Moore, J. VanderPlas, D. Laxalde, J. Perktold, R. Cimrman, I. Henriksen, E.A. Quintero, C.R. Harris, A.M. Archibald, A.H. Ribeiro, F. Pedregosa, P. van Mulbregt, SciPy 1.0 Contributors, SciPy 1.0: Fundamental Algorithms for Scientific Computing in Python, Nature Methods 17 (2020) 261–272, http://dx.doi.org/10.1038/s41592-019-0686-2.

[45] E. Hairer, G. Wanner, S.P.N. rsett, Solving Ordinary Differential Equations I, vol. 8, Springer Berlin Heidelberg, Berlin, Heidelberg, 1993, http://dx.doi.org/10.1007/978-3-540-78862-1.

[46] J.F. Donges, J. Heitzig, R.V. Donner, J. Kurths, Analytical framework for recurrence-network analysis of time series, Phys. Rev. E 85 (4) (2012) 1, http://dx.doi.org/10.1103/PhysRevE.85.046105.

[47] R.V. Donner, Y. Zou, J.F. Donges, N. Marwan, J. Kurths, Recurrence networks—a novel paradigm for nonlinear time series analysis, New J. Phys. 12 (3) (2010) 033025, http://dx.doi.org/10.1088/1367-2630/12/3/033025.

[48] R.V. Donner, Y. Zou, J.F. Donges, N. Marwan, J. Kurths, Ambiguities in recurrence-based complex network representations of time series, Phys. Rev. E 81 (1 Pt 2) (2010) 015101, http://dx.doi.org/10.1103/PhysRevE.81.015101.

[49] R.V. Donner, M. Small, J.F. Donges, N. Marwan, Y. Zou, R. Xiang, J. Kurths, Recurrence-based time series analysis by means of complex network methods, Int. J. Bifurcation Chaos 21 (04) (2011) 1019–1046, http://dx.doi.org/10.1142/S0218127411029021.

[50] N. Marwan, J.F. Donges, Y. Zou, R.V. Donner, J. Kurths, Complex network approach for recurrence analysis of time series, Phys. Lett. A 373 (46) (2009) 4246–4254, http://dx.doi.org/10.1016/j.physleta.2009.09.042.

[51] N. Marwan, C.M. Romano, M. Thiel, J. Kurths, Recurrence plots for the analysis of complex systems, Phys. Rep. 438 (5–6) (2007) 237–329, http://dx.doi.org/10.1016/j.physrep.2006.11.001.

[52] N. Marwan, K.H. Kraemer, Trends in recurrence analysis of dynamical systems, Eur. Phys. J. Spec. Top. 232 (1) (2023) 5–27, http://dx.doi.org/10.1140/epjs/s11734-022-00739-8.

[53] N. Marwan, A historical review of recurrence plots, Eur. Phys. J. Spec. Top. 164 (1) (2008) 3–12, http://dx.doi.org/10.1140/epjst/e2008-00829-1.

[54] D. Eroglu, N. Marwan, S. Prasad, J. Kurths, Finding recurrence networks' threshold adaptively for a specific time series, Nonlinear Proc. Geophys. 21 (6) (2014) 1085–1092, http://dx.doi.org/10.5194/npg-21-1085-2014.

[55] J.F. Donges, J. Heitzig, B. Beronov, M. Wiedermann, J. Runge, Q.Y. Feng, L. Tupikina, V. Stolbova, R.V. Donner, N. Marwan, H.A. Dijkstra, J. Kurths, Unified functional network and nonlinear time series analysis for complex systems science: The pyunicorn package, Chaos 25 (11) (2015) 113101, http://dx.doi.org/10.1063/1.4934554.

[56] J.F. Donges, H.C.H. Schultz, N. Marwan, Y. Zou, J. Kurths, Investigating the topology of interacting networks, Eur. Phys. J. B 84 (4) (2011) 635–651, http://dx.doi.org/10.1140/epjb/e2011-10795-8.

[57] F.D. Malliaros, M. Vazirgiannis, Clustering and community detection in directed networks: A survey, Phys. Rep. 533 (4) (2013) 95–142, http://dx.doi.org/10.1016/j.physrep.2013.08.002.

[58] G. Börner, H. Haehne, J. Casadiego, M. Timme, Revealing system dimension from single-variable time series, Chaos 33 (7) (2023) http://dx.doi.org/10.1063/5.0156448.

[59] H. Haehne, J. Casadiego, J. Peinke, M. Timme, Detecting hidden units and network size from perceptible dynamics, Phys. Rev. Lett. 122 (15) (2019) 158301, http://dx.doi.org/10.1103/PhysRevLett.122.158301.

[60] C. Geier, M. Stender, N. Hoffmann, Data-driven reduced order modeling for mechanical oscillators using koopman approaches, Front. Appl. Math. Statist. 9 (2023) http://dx.doi.org/10.3389/fams.2023.1124602.

[61] S.L. Brunton, J.L. Proctor, J.N. Kutz, Discovering governing equations from data by sparse identification of nonlinear dynamical systems, Proc. Natl. Acad. Sci. USA 113 (15) (2016) 3932–3937, http://dx.doi.org/10.1073/pnas.1517384113.

[62] J. Nawrath, M.C. Romano, M. Thiel, I.Z. Kiss, M. Wickramasinghe, J. Timmer, J. Kurths, B. Schelter, Distinguishing direct from indirect interactions in oscillatory networks with multiple time scales, Phys. Rev. Lett. 104 (3) (2010) 038701, http://dx.doi.org/10.1103/PhysRevLett.104.038701.

[63] Y. Zou, M.C. Romano, M. Thiel, N. Marwan, J. Kurths, Inferring indirect coupling by means of recurrences, Int. J. Bifurcation Chaos 21 (04) (2011) 1099–1111, http://dx.doi.org/10.1142/S0218127411029033.

[64] A. Groth, Visualization of coupling in time series by order recurrence plots, Phys. Rev. E 72 (4 Pt 2) (2005) 046220, http://dx.doi.org/10.1103/PhysRevE.72.046220.

[65] M. Thiel, M. Romano, J. Kurths, R. Meucci, E. Allaria, F. Arecchi, Influence of observational noise on the recurrence quantification analysis, Phys. D 171 (3) (2002) 138–152, http://dx.doi.org/10.1016/S0167-2789(02)00586-9.